# Analytical Methods

Accepted Manuscript


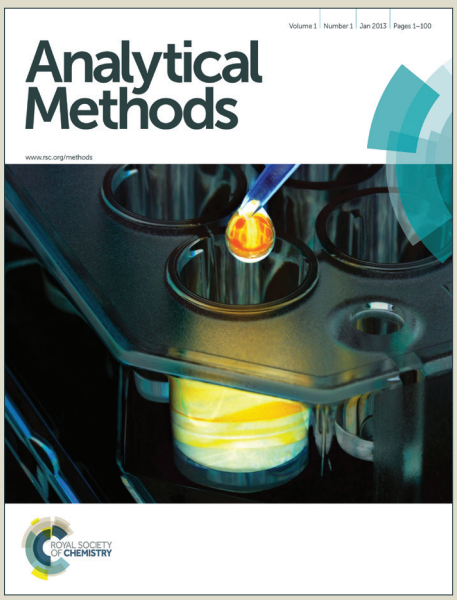





ROYAL SOCIETY OF CHEMISTRY

www.rsc.org/methods

# Functional Graphene- Gold Nanoparticles Hybrid System for Enhanced Electrochemical Biosensing of Free Cholesterol

*Shiju Abraham,[a] Narsingh R. Nirala,[b] Shobhit Pandey,[c] Monika Srivastava,[d] Sunil Srivastava,[e] Bernd Walkenfort[f] and Anchal Srivastava[a*]*

[a] *Department of Physics, Banaras Hindu University, Varanasi, 221005, India*

[b] *Department of Zoology, Banaras Hindu University, Varanasi-221005, India,*

[c] *Metallurgical Engineering Department, Indian Institute of Technology – (BHU)*

[d] *School of Materials Science and Technology, IIT (B.H.U.), Varanasi-221005, India*

[e] *Department of Pure and Applied Physics, Guru Ghasidas University, Main Campus,Koni, Bilaspur 495009, India*

[f] *Faculty of Chemistry, University of Duisburg, Essen, Germany*

ABSTRACT: Realizing the unavailability of fast and reliable diagnostics techniques, especially for cholesterol measurement, the present work reports the development of cost effective bioelectrodes based on reduced graphene oxide-functionalized gold nanoparticles (~25 nm) hybrid system (RGO-Fn Au NPs). The electrodes fabricated by electrophoretic deposition technique attest synergistically enhanced electro chemical sensing ability of 193.4 μA $mM^{-1}$ $cm^{-2}$ for free cholesterol detection, which is much higher than the traditional RGO system. The electrochemical impedance studies (EIS) show low charge transfer resistance, $R_{CT}$, for the hybrid system which is 57 % and 60 % lower than RGO and Au NPs respectively. Also higher loading capacity and enhanced kinetics has been realized for the hybrid system, owing to lower $K_m$ value (0.005 mM) and enhanced rate constant ($3.8 \times 10^{-4}$ cm $s^{-1}$) in comparison with RGO and Au NPs. Moreover, the RGO-Fn Au NPs platform promises wider range of cholesterol detection (0.65-12.93 mM), while simultaneously being able of detecting as low as 0.34 mM of free cholesterol. Apart from better sensitivity, loading capacity, kinetics and detection range, the system also has appreciable selectivity and stability. This supports its potential to be brought on field in the coming future for cost effective and reliable detection from complex system of human serum.

**Keywords:** Reduced graphene oxide, functionalized gold nanoparticles, cyclic voltammetry and cholesterol

**Address correspondence to:**

E-mail: anchalbhu@gmail.com (Dr. Anchal Srivastava)

Phone No.: +91-9453203122, Fax: +91-542 2368174

Hypercholesterolemia, which is a repercussion of the present generation eating habits, occurs when the cholesterol level in the body rises above the safe level of 200 mg $dL^{-1}$ (5.17 mM)[1]. Failing to efficiently diagnose the increased level of cholesterol in the human blood plasma results in fatal issues such as cardiovascular diseases, coronary artery diseases, transient ischemic heart attacks and atherosclerosis[2,3]. This demands a better and efficient system which can work selectively in the complex system of blood, being affordable at the same time. The traditional chemical approaches for the analysis of cholesterol such as colorimetry, fluorimetry, gas chromatography/mass spectrometry and spectrophotometry suffer from common drawbacks such as low selectivity and specificity due to masking of the main chemical reaction with the interfering side reactions. This is further aggravated by the involvement of unstable and corrosive reagents[4]. On the contrary, electrochemical-enzymatic biosensing procedures, unlike chemical methods show good specificity and selectivity for determination of free cholesterol and other analytes in biological samples[5,2].

It is important for the a bioelectrode system to have better physico-chemical, catalytic and surface properties in order to ensure high loading of the analytes, enhanced electron transfer rate and several fold increase in signal to noise ratio. Fulfilling these requirements, nanostructures based electrochemical biosensors were the first to have received wide attention in the last decade with the added advantage of portability and inexpensiveness[6,7]. Among the prominent candidates, gold nanoparticles (Au NPs), which have been extensively used in diverse biological applications owing to their appreciable biocompatibility, is the most promising one[8]. These noble nanoparticles have unique properties such as the plasmonic properties, large surface area for larger loading of reactive molecules per particle and low cytotoxicity, which is why they have been applied in diagnostics and therapeutic work like labelling, delivery, sensing, and photo thermal therapy[9–11].

Above stated requirements for an efficient biosensor soon paved the way for graphene family as yet another promising biosensing system owing to its ultra- high surface area and peculiar electronic properties[12,13]. Among the successful candidates in graphene family, reduced graphene oxide (RGO) based systems have shown appreciable potential for the detection and monitoring of different biomolecules[14,15]. This is due to their enhanced electrochemical activities, bulk production ability, enlarged conductivity, and high 2-D surface area along with sufficient functional groups. Although RGO, with restored conductivity can perform comparatively well alone, however highly improved electrochemical activities and enhanced sensitivity is reported when it is used as a matrix

to combine with metal and metal oxide nanoparticles to form efficient hybrid systems. This diversifies and improves its applicability as required for current needs[16–18]. Specially, the importance of combining RGO with Au NPs is prototypical providing better properties which have been utilized for biosensing recently, for eg. the detection of dopamine [19] and glucose sensing[20].

Hence acknowledging the potential of fabricating metal nanoparticles-RGO hybrid system, the present work proposes efficient reduced graphene oxide-functionalized gold nanoparticles (RGO-Fn Au NPs) composite system for efficient free cholesterol sensing. For a comparative study the present work fabricates thin film of both RGO and RGO-Fn Au NPs hybrid system separately on indium tin oxide (ITO) coated glass substrate. Additionally, electrophoretic deposition technique (EPD) used for these electrodes fabrication is both cost effective and shows bulk production potential. This can be understood by as low as ~0.2$ estimated cost for single bioelectrode produced in our work. Typically, when immobilized by cholesterol oxidase (ChOx) for cholesterol detection via cyclic voltametry (CV) technique, RGO-Fn Au NPs based electrode shows enhanced electro chemical sensitivity in comparison to RGO. Finally this ecological system's potential to be applied on field is attested by its good biocompatibility, non-toxic nature and particularly its high stability as expected by chemically stable combination of RGO and Fn Au NPs in their composite form[21–23]. With these advantages, the system proves itself as a promising biosensing system which can be brought on field in coming future.

## EXPERIMENTAL SECTION

**Materials.** Graphite flakes (NGS Naturgraphit GmbH, Germany), Tetrachloroauric acid ($HAuCl_4$), $H_2SO_4$, $H_3PO_4$, $KMnO_4$, $H_2O_2$, Hydrazine Hydrate, ammonia solution, ethanol, etc.used were of technical grade. All the chemicals employed for the fabrication of cholesterol biosensor, namely, cholesterol oxidase (ChOx), cholesterol, etc. were procured from Sigma-Aldrich.

**Preparation of Graphene Oxide (GO), Reduced Graphene Oxide (RGO), Gold Nanoparticles (Au NPs) and their functionalization:** GO has been synthesized by the method proposed by Marcano et al[24,7] {see supplementary information}. RGO has been prepared by following the chemical method proposed by Dan Li et al[25]. Further gold nanoparticles were prepared by the trisodium citrate reduction of gold precursor[26]. For the functionalization, 10 mL of Au NPs after centrifugation were re-suspended in 10 mL of DW as the first step. This Au NPs solution was then

treated with 1 mL of MUDA ($C_{11}H_{22}O_2S$, 20 mM) in ethanol and subsequently 5 mL of DW was added to it. This combination was sonicated at 50° C for an hour and kept undisturbed for one day to obtain Fn Au NPs.

**Fabrication of RGO- Fn Au NPs thin film electrodes.** First, the RGO-Fn Au NPs Hybrid system was prepared using combination of sonication and stirring at specific temperatures {see supplementary information}. Thin film of nanostructured RGO as well as RGO-Fn Au NPs (2 mg $dL^{-1}$ in acetonitrile) were then fabricated over ITO electrodes via EPD technique. Typically, a pre-cleaned ITO-coated glass substrate having sheet resistance of 30 Ω $cm^{-1}$ was used as the working electrode and a platinum foil (1 cm × 2 cm) was used as the counter electrode. Keeping these electrodes parallel to each other in the desired RGO and RGO-Fn Au NPs colloidal suspension, thin film of RGO and RGO-Fn Au NPs was deposited on the ITO-coated glass plates respectively. These thin film coated electrodes were then removed from the suspension, washed with deionized water and dried.

**Solution preparation and immobilization.** A stock solution of 500 mg $dL^{-1}$ (12.93 mM) of cholesterol was prepared by dissolving cholesterol in a flask containing Triton X-100 placed in a heat bath of 60 ℃. This stock solution was further diluted with 0.02 M PB solution (pH 7.0) for making different cholesterol concentrations (25 mg $dL^{-1}$ to 500 mg $dL^{-1}$). RGO as well as RGO-Fn Au NPs electrode's COOH groups were activated using the EDC-NHS coupling chemistry. For the immobilization of ChOx onto RGO/ITO and RGO-Fn Au NPs/ITO, a 5 µl of ChOx (Cholesterol oxidase (EC1.1.3.6 ≥50 U $mg^{-1}$) was used to cast a film over the electrodes. These bioelectrodes were allowed to dry at 4 ℃ in a refrigerator. These activated electrodes were then washed thoroughly using PB solution (pH ~7) and stored at 4 °C in dry state until use. The MUDA molecule in the Au NPs possess acid group on its edges providing extra binding points to the enzyme.

**Characterization of the materials.** The structural characterization of RGO and RGO-Fn Au NPs was done by X-ray diffraction (XRD) technique (D8 ADVANCE, Bruker). The wavelength of Cu-Kα1 radiation of λ=1.5405 Å was used for obtaining the XRD pattern. The morphological changes were investigated employing scanning electron microscope [FE-SEM (Zeiss, Merlin)] instrument operated at an accelerating voltage 20 V to 30 kV. The transmission electron microscope (TEM) images were obtained using a Zeiss EM 902 instrument. The UV−vis absorption measurements were

carried out with a Cary 5000 UV−vis absorption spectrometer from Varian employing the double beam mode. Fourier transform infrared (FT-IR) spectroscopy (Perkin Elmer Spectrum 65, FT-IR spectrometer) was employed for the identification of molecular structures. The Raman measurements were performed on a micro-Raman setup (HR LabRam inverse system, Jobin Yvon Horiba) using the 532 nm line from a frequency doubled Nd:YAG laser (Coherent Compass. Electrochemical studies (cyclic voltammetry) related to cholesterol detection have been carried out on Autolab Potentiostat/ Galvanostat. Electrochemical impedance spectroscopy (EIS) for the electrodes was measured between the frequency range 100 kHz to 1 Hz with a 5 mV amplitude using an applied potential of 0.2 V.

## RESULTS AND DISCUSSION

**Structural and spectroscopic studies.** X-ray diffraction (XRD) pattern was used to fingerprint the RGO-Fn Au NPs (see supplementary information, Figure S3). The XRD pattern of RGO exhibits an intense peak around 24.5°, which corresponds to the (002) plane, and, a weak peak around 10° due to the contribution from unreduced graphene oxide.[27] This $d_{002}$ value along with the broadness of the reflection supports the restacking of graphene sheets due to the loss of oxygen-containing functional groups during the reduction process. Using Bragg's law, the value of the d-spacing is calculated as 0.35 nm, for the diffraction peak at 24.5°. The other four peaks of 2Θ at 38°, 44°, 64° and 78° correspond to the Au NP's reflections at (111), (200), (220) and (311) respectively.[28]

Figure 1 shows the SEM micrographs of the RGO, Au NPs and RGO-Fn Au NPs. Fig. 1 (a) represents the RGO nanosheets with their typical wrinkles and foldings. Further the two dimensionality of RGO extending to several micrometers without losing uniformity can be observed. Fig. 1 (b), indicates Au NPs having particle size of ~25 nm, which sit on the $Si/SiO_2$ substrate with appreciable uniformity. As expected due to less adhesion of Au NPs with the $Si/SiO_2$ substrate, the particle density on the substrate is less. Sensitive backscattered electron (BSE) detectors are used to visualize a rich qualitative compositional contrast and internal structure information with similar resolution to that of secondary electrons (SE) detectors. Fig. 1 (c) shows the BSE micrograph of RGO-Fn Au NPs. Here the Au NPs are strikingly identified owing to their enhanced contrast with respect to the fade RGO background. The Fig. 1 (d) shows the micrograph of RGO-Fn Au NPs hybrid system for a relatively longer region. The image illustrates the uniform distribution of the Au NPs which were adsorbed nicely on the surface of RGO. Again in contrast to $Si/SiO_2$ substrate, the

Au NPs density on RGO is quite high owing to good adhesion property between RGO and Au NPs. EDX diagram can be seen in the inset figure confirming the elemental analysis of the RGO-Fn Au NPs system. As expected mainly carbon, oxygen and gold were present in the composite system supporting the purity of the formed composite. The sodium content presence in the spectrum is due to the unreacted reducing agent; trisodium citrate used for Au NPs synthesis and also may be from the quality of acids used for the synthesis of graphene oxide.

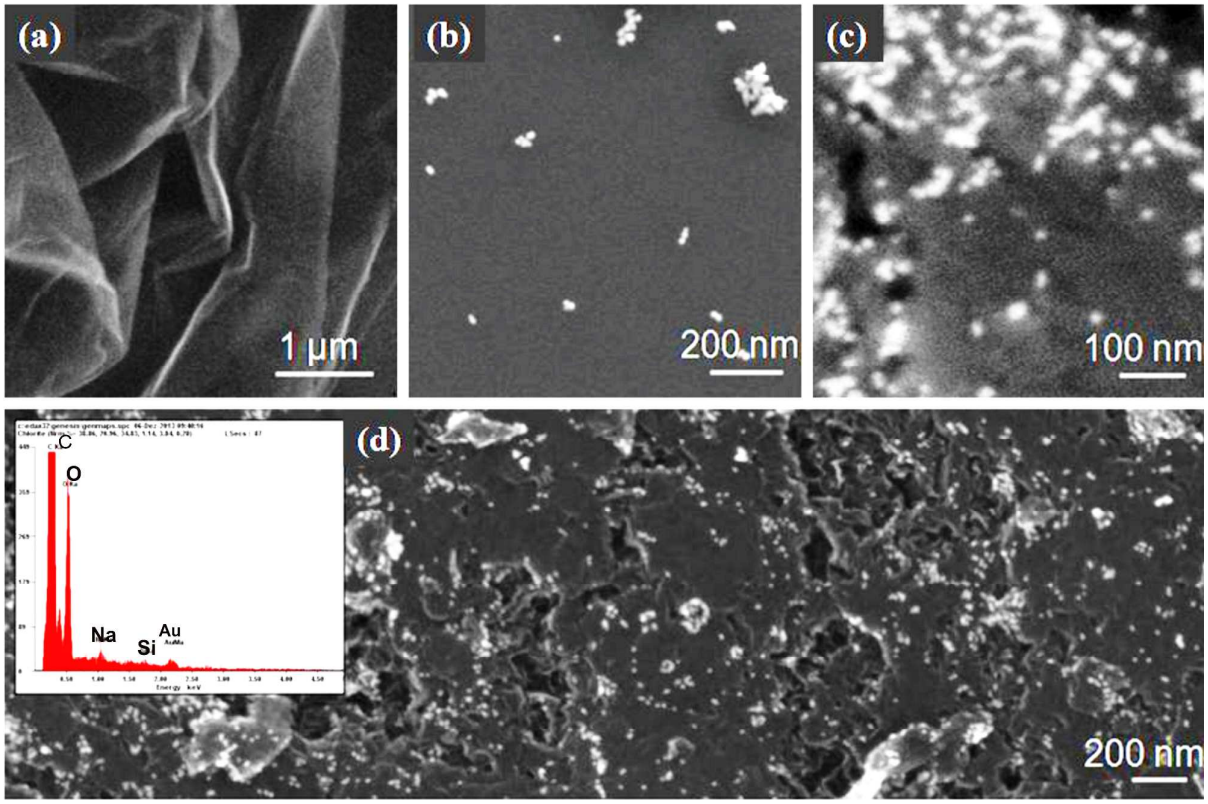


***Figure 1.*** *Scanning Electron Microscopic (SEM) images of; (a) RGO nanosheets with folding and micrometers of uniformity in lateral dimensions; (b) Au NPs with average size distribution of ~25 nm; (c) back scattered image of RGO-Fn Au NPs which shows clear contrast of Au NPs with respect to RGO sheets; (d) RGO-Fn Au NPs composite system with long range uniformity showing a nice distribution of Au NPs over as well as on the folding and defects of RGO. The inset shows the EDX of the RGO-Fn Au NPs composite system showing the elemental combination of Carbon, Oxygen as well as Au.*

TEM results of RGO, Au NPs and RGO-Fn Au NPs are depicted in Figure 2. Few layered RGO nanosheets of long homogeneity with several nanometers-long wrinkles are visible in Fig. 2(a).

Fig. 2 (b) shows the TEM micrograph of Au NPs of ~25 nm in a more distinguishable manner, showing their almost spherical and oval shape. Fig. 2(c) indicates the RGO-Fn Au NPs system where, Au NPs are well decorated on the RGO surfaces with some of them encapsulated by the RGO sheet.

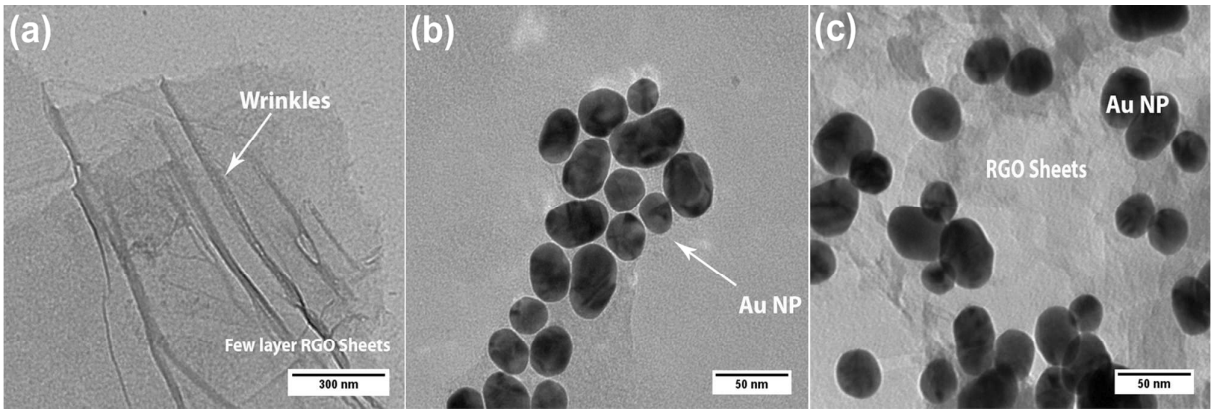


***Figure 2.*** *Transmission Electron Microscopic (TEM) images of; (a) RGO nanosheets of few layers with wrinkles and folding; (b) Au NPs with average size of ~25 nm; the shape of the particles are spherical and oval in nature. (c) RGO-Fn Au NPs hybrid system with Fn Au NPs nicely attached to the surfaces and foldings of few layered RGO nanosheets.*

Raman spectroscopy is a well-known, non-destructive technique to distinguish between $sp^2$ and $sp^3$ hybridization in carbonaceous materials as well as to identify the number of layers present in graphene.[29–32] The two main characteristic Raman bands present in almost all carbon-based materials are the G-band and D-band. Figure 3 represents the optical micrograph and Raman mapping of RGO-Fn Au NPs taken in an area of 140 × 140 μm to have precise information about the chemical homogeneity on a larger scale. As the Au NPs do not show any significant signature in the composite system, the mapping shows information regarding the intensity distribution of different bands observed in RGO. Fig. 3(a) shows the optical micrograph of the RGO-Fn Au NPs sheets on a glass substrate. Fig. 3(b) shows the raman spectrum of the sample. Here, an intense G-band and prominent D as well as 2D band can be observed. It is clearly visible that the intensity ratio of $I_{2D}/I_G$ is less than 1 (~0.4), which is an indication of systems decreased disorderness and better reduction while forming the composite. This also suggests that definitely a single layer reduced graphen oxide is not formed in the electrode, however, the full width at half maximum (FWHM) for the 2D band attests that the number of layers is restricted to ~5 or even less. The calculated FWHM at 2704 $cm^{-1}$ is ~68.$cm^{-1}$, and according to the report of Hao et.al[33], FWHM broadens with increasing number of layers, reaching a value of 66.1 ± 1.4 $cm^{-1}$ for five layers of graphene, which almost matches with the

calculated FWHM in our case. Alternatively, this broadening of FWHM (in comparison to ~27.5 ± 3.8 $cm^{-1}$ FWHM for single layer) could also be attributed to the presence of non-uniform number of layers which affects the double resonance process leading to such levels of broadening even when combination of bi-layer and few layers is present. Fig. 3(c) shows the D-band region (1300-1380 $cm^{-1}$). While some areas in the mapping show the presence of dense intensity distribution, the other areas have homogeneous distribution of disorderness. The dense areas indicate the oxidized regions of GO and the disorder induced through presence of functionalized gold nanoparticles. Fig. 3(d) shows the G-band region (1550-1610 $cm^{-1}$). The corresponding intensity distribution map is in accordance with the optical image, indicating systems purity. Fig. 3(e) indicates the 2D-band region (2650-2750 $cm^{-1}$), which is well pronounced, confirming RGO's few layered nature as attested by the considerable intensity for the 2D band to give the ratio $I_{2D}/I_G$ an appreciable value (~0.4)[29].

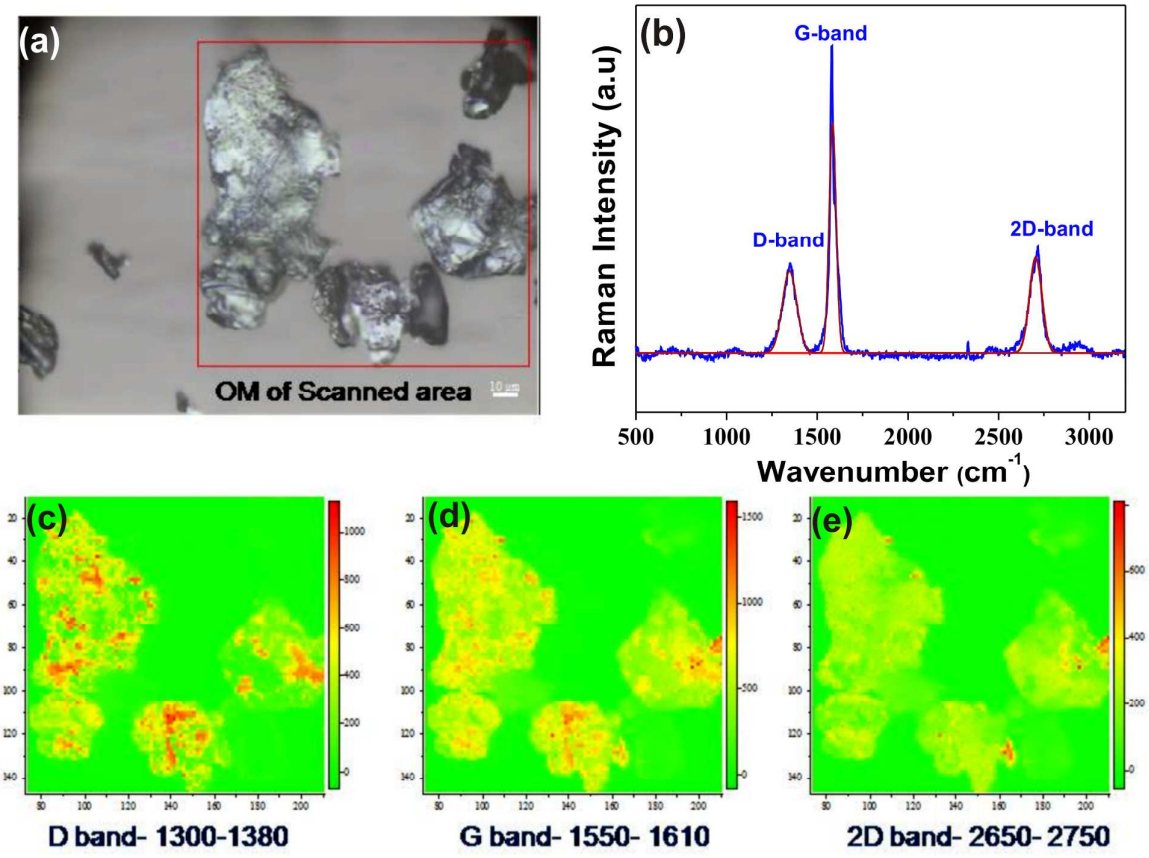


***Figure 3.*** *Raman mapping of RGO-Fn Au NPs taken at scanning area of 140×140 µm using an excitation source of 532.5 nm; (a) Optical micrograph of the scanned area; (b) Raman spectra of RGO-Fn Au NPs; Raman intensity mapping for the (c) D-band region (1300-1380 $cm^{-1}$) (d) G-band region (1550-1610 $cm^{-1}$) (e) 2D-band region (2650-2750 $cm^{-1}$)*

**Electrochemical characterization and cholesterol sensing.** Amperometric biosensors work by the production and monitoring of current on the application of potential between two electrodes. In mediated biosensors enzymes donate electrons to mediators or electrochemically active artificial electron acceptors, which are effective in reducing the electrochemical interferences. The process requires the cycle of enzyme - substrate redox reaction followed by re-oxidization by the mediator. The electrodes measure the concentration of $O_2$ or the product $H_2O_2$ in the enzymatic reaction.

The schematic representation of electrochemical sensing set up used for cholesterol sensing is shown in Figure 4. In this schematic, part (a) shows the EPD set up used for the fabrication of both RGO as well as RGO-Fn Au NPs electrodes. One of the produced electrode, i.e, RGO-Fn Au NPs thin film electrode on ITO coated glass substrate is shown in part (b), displaying the presence of functional groups. Part (c) shows the ChOx enzyme immobilization on RGO-Fn Au NPs through EDC-NHS coupling reaction. The resulting ChOx immobilised bioelectrode and the electrochemical reactions are illustrated in part (d). Known concentration of cholesterol is added to the electrochemical cell containing three electrodes. The cell comprises of RGO/ChOx/ITO or RGO-Fn Au NPs/ChOx/ITO bioelectrodes as the working electrode, platinum foil as the counter electrode and Ag/AgCl as a reference electrode in 50 mM phosphate buffer saline (PBS) of pH 7.0 containing 5 mM of $[Fe(CN)_6]^{3-4-}$. The current produced from the electrochemical reaction is interfaced through a Potentiostat/Galvanostat and finally the signals are interfaced to the computer.

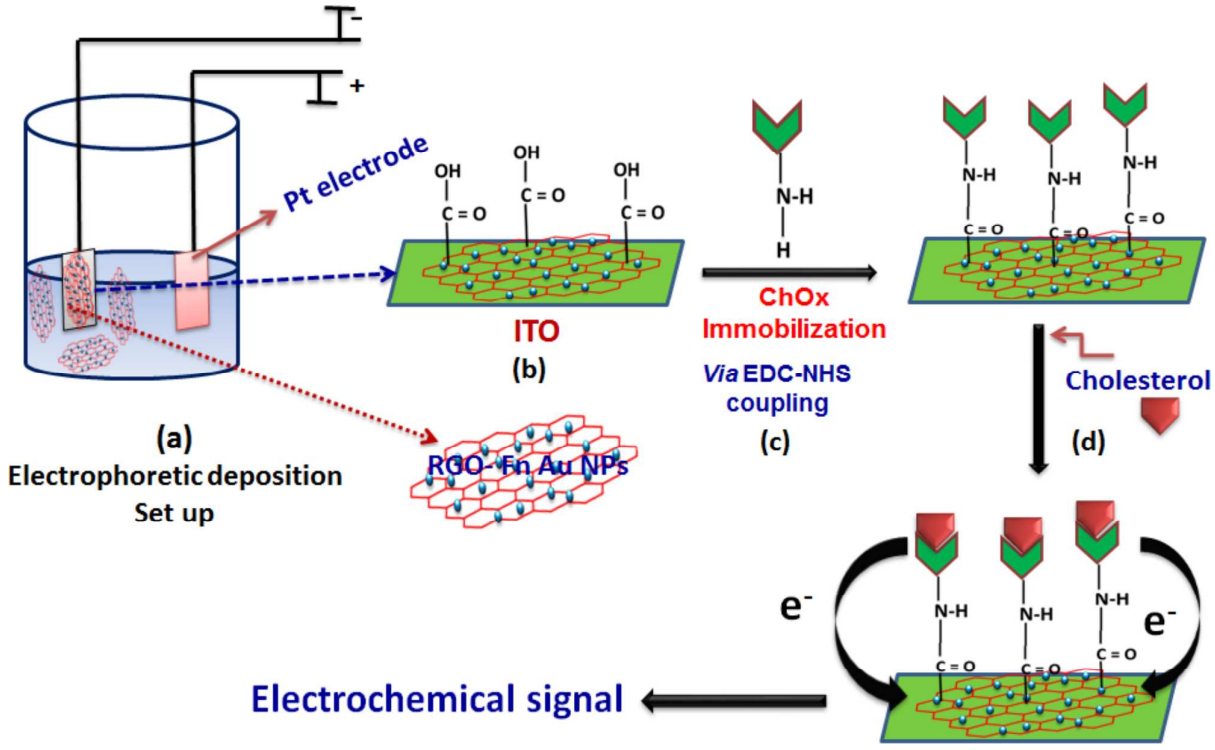

***Figure 4.*** *Schematic representation of cholesterol sensing process: EPD set up for the fabrication of RGO and RGO-Fn Au NPs thin films; (b) electrophoretically fabricated RGO-Fn Au NPs thin film on ITO substrate; (c) immobilization of ChOx on RGO-Fn Au NPs by EDC-NHS coupling; (d) the immobilized RGO-Fn Au NPs bioelectrode and the electrochemical reaction while adding cholesterol to the electrochemical cell contain the bioelectrode.*

The cyclic voltammogram (CV) studies of ITO, RGO/ITO, RGO-Au NPs/ITO, RGO/ChOx/ITO and RGO-Au NPs/ChOx/ITO electrodes, in PBS (pH ~7) containing 5 mM $[Fe(CN)_6]^{3-/4-}$ is shown in Fig. 5(A). Oxidation peak current of 0.53 mA corresponding to the bare ITO based electrode is observed. However, the current increases to 0.77 mA in the case of RGO/ITO electrode owing to its good electrical conductivity as well as the ability to function as a good platform for electron transfer. RGO-Fn Au NPs/ITO system shows much enhanced current (0.92 mA) than RGO/ITO due the synergistically enhanced electro catalytic activity on combining Au NPs with RGO. After the ChOx immobilization with RGO/ITO, the response current gets reduced to 0.59 mA and in case of ChOx/RGO-Fn Au NPs/ITO, it comes down to 0.65 mA.

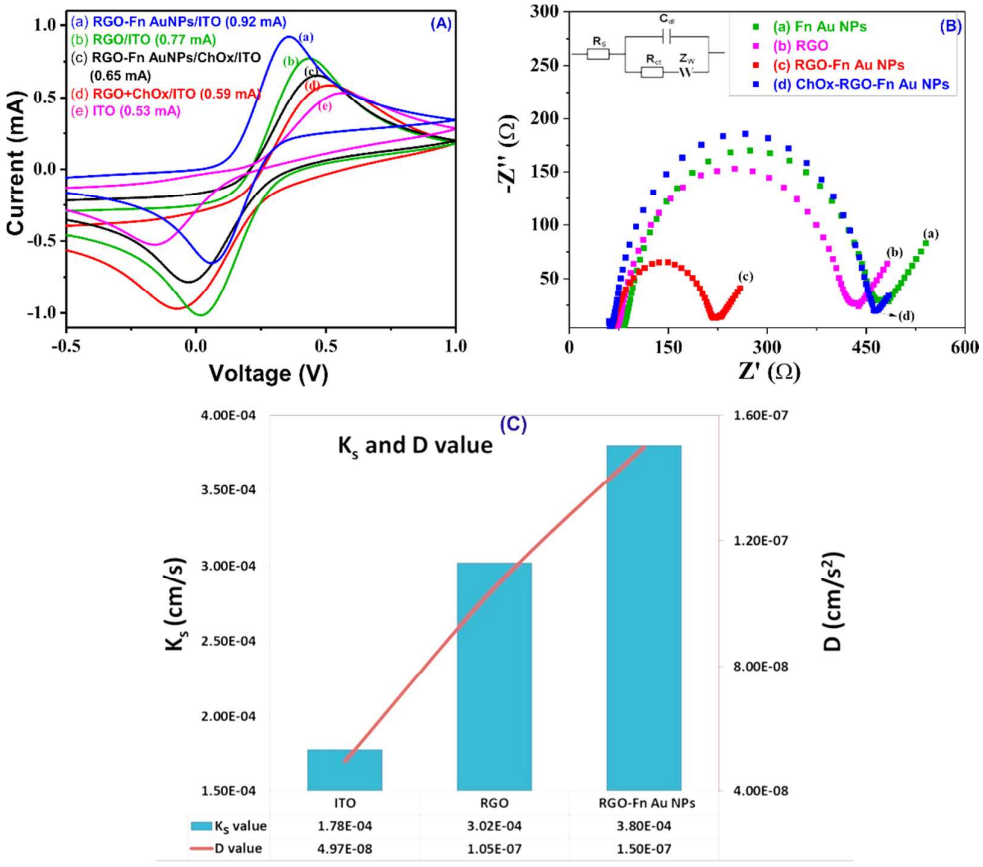

***Figure 5.*** *(A) CV Response of (a) RGO-Fn Au NPs/ITO; (b) RGO/ITO; (c) RGO-Fn Au NPs/ChOx/ITO; (d) RGO/ChOx/ITO; (e) ITO electrode; (B) Nyquist plot of RGO, Au NPs, RGO-Fn Au NPs and RGO-Fn Au NPs/Ch-Ox electrodes in PBS (pH= 7) containing 5mM* $[Fe(CN)_6]^{3-/4-}$*; (C) Bar plot of parameters* $K_s$ *and D for ITO, RGO and RGO-Fn Au NPs electrodes.*

Here in these bioelectrodes, the redox active sites are deeply embedded in the ChOx bienzymes macromolecular structure. The insulating characteristics of these enzymes explains the above mentioned reduction in current when compared to their non-immobilized counterpart. However, the dominant behavior of composite system persists. Further due to reduced conductivity of these bioelectrodes, the oxidation peak potential shifts towards higher positive value as compared with the non-immobilised electrodes.

The Electrochemical impedance is observed when current flows through a circuit consisting of resistors and capacitors or inductors. The equivalent circuit which can be used to measure the electrochemical impedance, ie. the Randles circuit [Inset Fig. 5(B)] is composed of solution resistance $R_S$, charge transfer resistance $R_{CT}$ and double-layer capacitance $C_{dl}$ or constant phase element (CPE)[34]. The Nyquist plot used to find the $R_{CT}$ for all electrodes is shown in Fig. 5(B). The semicircle diameter, which indicates the magnitude of the $R_{CT}$ is associated with the dielectric and insulating characteristics across the electrode/electrolyte interface. The RGO electrode shows a $R_{CT}$ value of 350 Ω, whereas, Au NPs shows 383 Ω of $R_{CT}$ value. However, in case of the hybrid system, i.e. RGO- Fn Au NPs, the $R_{CT}$ value is as low as 151 Ω as denoted by the smallest semi-circle. This supports the fast charge transfer kinetics of RGO- Fn Au NPs as compared to RGO as well as Au NPs, following higher separation efficiency of electrons and holes. Further, as expected, the $R_{CT}$ value of this composite system increases to 399 Ω after immobilization with ChOx owing to lower conductivity of ChOx. Evidently, the increase in $R_{CT}$ value indirectly supports the binding of ChOx onto RGO- Fn Au NPs.

Fig. 5(C) further supports RGO- Fn Au NPs dominance over RGO for faster electron transfer by having much higher diffusion coefficient (D)[35] and standard heterogeneous rate constant ($K_s$) calculated using Klingler and Kochi[36] equation, i.e. Eq. (1).

$$K_S = 2.18\sqrt{\left(\frac{D\alpha nFv}{RT}\right)}\, exp\left[-\frac{\alpha^2 nF}{RT}\left(E_{p-}^{a} E_p^{c}\right)\right] \cdots\cdots (1)$$

$$i_p = Constant\ nFAC\sqrt{(\frac{nFvD}{RT})}\} \cdots\cdots (2)$$

In above equations, R is universal gas constant, F is Faraday Constant in C $mol^{-1}$, α is transfer coefficient (For ITO: α = 0.165, RGO /ITO: α = 0.215 and RGO –Fn Au NPs/ITO : α = 0.268), $E_p$ is oxidation peak potential, ν is scan rate and T is the temperature in Kelvin. In present study, the D value was determined using Randles-sevcik equation. Here the RGO- Fn Au NPs shows a higher D value of $1.5 \times 10^{-7}$ $cm^2$ $s^{-1}$ and $K_s$ value of $3.8 \times 10^{-4}$ cm $s^{-1}$ whereas bare ITO show the least D and $K_s$ values, $4.97 \times 10^{-8}$ $cm^2$ $s^{-1}$ and $1.7 \times 10^{-4}$ cm $s^{-1}$ respectively. Consistently, the RGO electrode showed an intermediate D and $K_s$ values of $1.05 \times 10^{-7}$ $cm^2$ $s^{-1}$ and $3.02 \times 10^{-4}$ cm $s^{-1}$ respectively. These enhanced D and $K_s$ value for RGO- Fn Au NPs is aroused due to the synergistic effect of conductive 2-dimensional RGO sheets in combination with the good catalytic effect of Au NPs. These calculations further attest the selection of such a hybrid system as a much suitable electrode material for the fabrication of highly sensitive and selective cholesterol biosensor.

Electrochemical response studies of RGO/ChOx/ITO and ChOx/RGO-Fn Au NPs/ITO have been summarized in Figure 6. The measurements were carried out as a function of cholesterol concentration using cyclic voltammetry in PBS solution {50 mM PBS (pH 7, 0.9% NaCl) containing 5 mM $[Fe(CN)_6]^{3-/4-}$}. The observations show an increase in the magnitude of current for the bioelectrodes as the concentration of cholesterol was increased (from 25 mg $dL^{-1}$ to 500 mg $dL^{-1}$) in case of both ChOx/RGO/ITO and ChOx/RGO-Fn Au NPs/ITO bioelectrodes. Fig. 6(a) shows the CV response voltage *vs* current plot of ChOx/RGO/ITO and the curves from 'a' to 'h' indicate different concentrations of cholesterol from 25 to 500 mg $dL^{-1}$ which include the following concentrations; 25, 50, 100, 150, 200, 300, 400 and 500 mg $dL^{-1}$. In Fig. 6(b) fitting of the calibration plot relating the anodic peak current and cholesterol concentrations for RGO/ITO shows a distinct linear region within the concentrations range of 50-500 mg $dL^{-1}$. Using this several electrochemical sensing paramters can have been calculated. The detection range for the RGO/ITO bioelectrode comes out to be 25 – 500 mg $dL^{-1}$ (0.65 mM-12.93 mM) with a detection limit of 10 mg $dL^{-1}$ (0.26 mM); low enough to measure the cholesterol level in human serum. The criteria used for the calculation of detection limit is of 3σ/m, where 'm' is the slope and 'σ' is standard deviation (SD) of the calibration graph. Further, the sensitivity of RGO/ITO bioelectrode is found to be 116 μA $mM^{-1}$ $dL^{-1}$ which itself is better than several earlier reports (See Table No. 1). Further, the accuracy of fitting curve can be acknowledged by as low as 0.9952 value of the regression coefficient '$R^2$'. Fig. 6(c) shows the CV response of RGO-Au NPs/ChOx/ITO for the cholesterol concentrations 25 to 500 mg $dL^{-1}$ denoted by the curves 'a' to 'h'. Clearly the magnitude of current difference between ChOx/RGO-Fn Au NPs/ITO is higher than ChOx/RGO/ITO system. The fitted calibration plot for ChOx/RGO-Fn Au NPs/ITO shows its linear behavior from 25-500 mg $dL^{-1}$ as shown in Fig. 6(d).

The linear range in this case is better than that of ChOx/RGO/ITO and so are the sensing parameters. The ChOx/RGO-Fn Au NPs/ITO system shows a lower detection limit of 13 mg $dL^{-1}$ (0.33 mM) fitted perfectly with '$R^2$' value of 0.9941. Additionally, an enhanced sensitivity of 193.35 μA $mM^{-1}$ $dL^{-1}$ is observed in this case which supersedes that of bare RGO/ITO bioelectrode. This improvement is credited to the synergistic presence of the Au NPs along with RGO matrix in improving the electrochemical properties.

Additionally, ferri/ ferrocyanide was used as an inorganic mediator to work as an artificial electron transferring agent. This mediator can readily participate in the redox reaction with the biological molecule and boost the electron transfer. The specialty of these mediators lie in their ability to regenerate close to the electrode surface via electrochemical reaction thereby enabling the electrochemical reaction to take place at the characteristic potential of the mediator. Even in the presence of only small amount of biological molecules, the current enhances significantly signifying a rapid chemical reaction. Hence clearly, as the fundamental premise, in this cholesterol sensing process, the observed current is related to the concentration of the biomolecule present (here cholesterol). The enzymatic reaction is as follows:

$$Cholesterol + 2[Fe(CN)6]^{3-} + H_2O \xrightarrow{ChOx} Cholestenone + 2H^+ + 2[Fe(CN)6]^{4-} \cdots\cdots (3)$$

$$[Fe(CN)6]^{4-} \xrightarrow{\text{ChOx– RGO–Fn Au NPs/ITO}} [Fe(CN)6]^{3-} + e^{-1} \cdots\cdots (4)$$

During the above biochemical reaction (shown in Eq. 3 and 4), ChOx catalyzes in the presence of oxygen and cholesterol gets oxidized to cholestenone and $H_2O_2$. The $O_2$ in this reaction originates from the PBS buffer solution. The electro oxidation current of $H_2O_2$ can be monitored by applying a suitable potential to this system. The extra potential required for the oxidation/ reduction of $H_2O_2$ can be reduced by immobilizing the ChOx enzyme in a suitable immobilization matrix. Here the RGO/ITO and RGO-Fn Au NPs/ITO is found to be one of the best suitable and cost effective matrixes to serve the same purpose. During the electrochemical reaction, the electrons generated will be transferred to the electrodes via an Fe(III)/ Fe(IV) redox probe that will result in translation of the signal in the form of current. So in this process, the corresponding increase in current is a direct indication of total cholesterol added to the system.

Michaelis–Menten constant ($K_m$), a well known enzyme and substrate kinetics parameter has been estimated for the bioelectrodes in present work using the Lineweaver–Burke plot[37] revealing

the strong affinity of the enzyme towards the desired analyte. The $K_m$ value has been calculated using Eq. (5).

$$\frac{i}{i_s} = \frac{k_m}{i_{max}} \frac{1}{C} + \frac{1}{i_{max}} \cdots\cdots (5)$$

Where, 'C' is the concentration of mediator in mol/cm$^3$, '$i_{max}$' is the maximum peak current and '$i_s$' is the starting current. Calucluated value of $K_m$ for the ChOx/RGO/ITO bioelectrode is 0.4 mg dL$^{-1}$ (0.01 mM) while for ChOx- RGO-Au NPs/ITO, it is 0.2 mg dL$^{-1}$ (0.0051 mM); smaller than most of the earlier reports (Table.1). Such low $K_m$ value of ChOx- RGO-Au NPs/ITO suggests that the electrode matrix used here helps immobilized cholesterol oxidase to achieve a better conformation for faster enzymatic reaction. Thus, the ChOx- RGO-Au NPs/ITO provides a better platform for electron transfer between the immobilized enzyme and the electrode substrates and plays the major role in enhancement of electrochemical response. These results has been further corroborated by DFT calculations, which attests enhanced electron density distribution for RGO-Au NPs system in comparison with bare RGO system. (see supplementary information).

To investigate the viability of as fabricated biosensor, we have conducted the reproducibility, specificity and stability measurements and the results further confirm RGO-Fn Au NPs/ITO as a promising candidate in biosensing, which combines the advantages of both graphene as well as metal nanoparticles of gold, which themselves are good biosensing materials.

The specificity of cholesterol towards RGO-Fn Au NPs/ChOx/ITO bioelectrodes along with other analytes has been checked. Negligible effect of interference on the corresponding peak current response of RGO-Fn Au NPs/ChOx/ITO biosensor inspite of the presence interferents such as glucose (100 mg dL$^{-1}$), ascorbic acid (0.05 mM) and urea (1 mM) in phosphate buffer (0.2 M, pH 7.0), marks its high selectivity for effectively detecting cholesterol, which is important for the material to perform appreciably in complex human serum {supplementary information, Fig. S5(a)}. The stability of the RGO-Fn Au NPs/ChOx/ITO biosensor is monitored for nine weeks by measuring peak current response with respect to time at a regular interval of one week. The RGO-Fn Au NPs/ChOx/ITO biosensor has shown a slightly decreased peak current response (~9.2%) after nine weeks when stored in refrigerated conditions (4 °C). {Supplementary information, Fig. S5(b)}. This shows the good stability of fabricated biosensor for a longer period of time and which in turn shows its potential to be brought on field with no degradation issue during transportation and long term use. Similarly, the reproducibility of the bioelectrodes of RGO-Fn Au NPs/ChOx/ITO used for the fabrication of cholesterol biosensors has been determined in terms of peak current response. For checking this, five different RGO-Fn Au NPs/ChOx/ITO bioelectrodes have been prepared under the

same set of condition and procedure. No appreciable change in peak current response was recorded confirming its high reproducibility.{see supplementary information, Fig. S5(c)}.

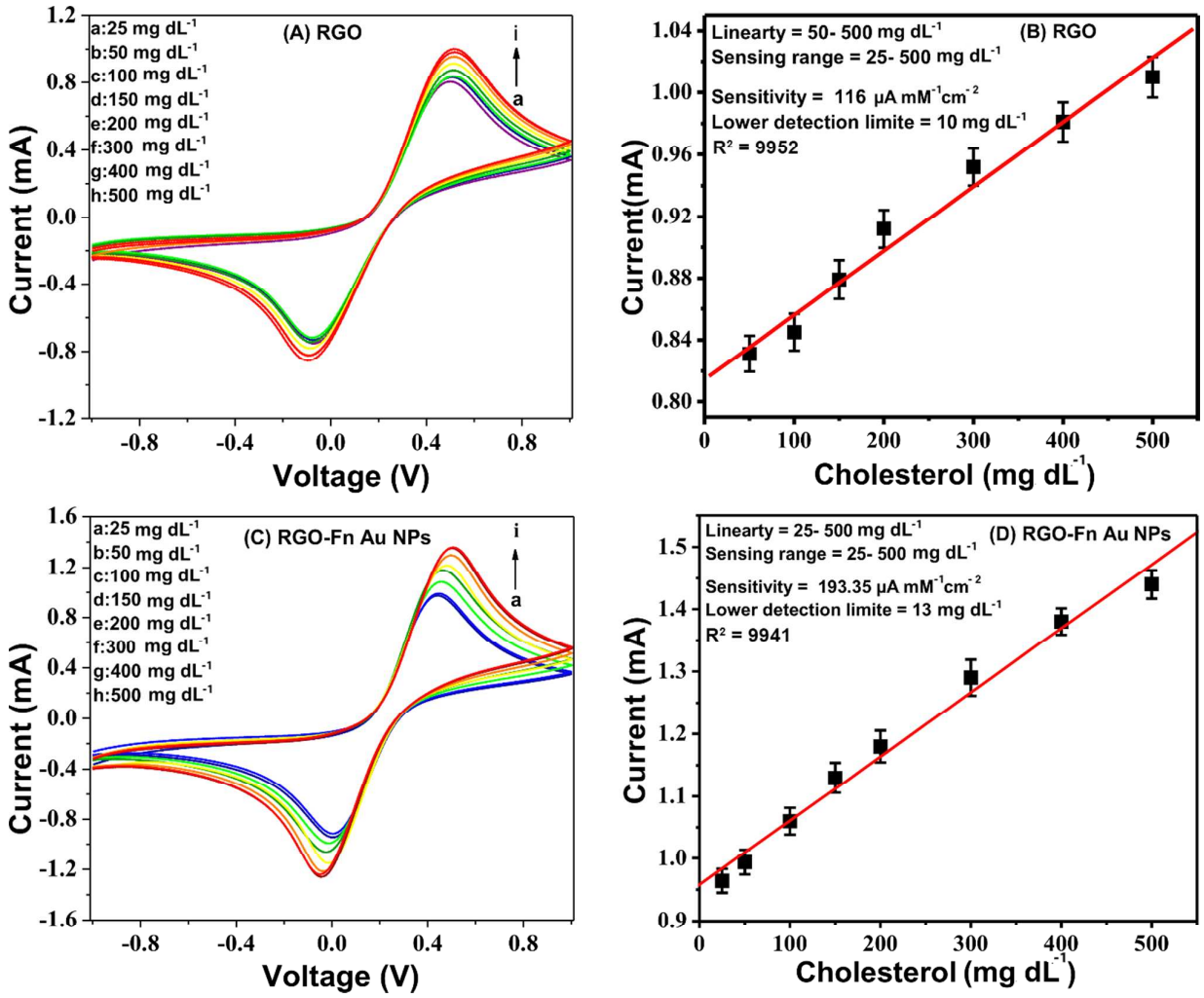


***Figure 6.*** *Electrochemical response studies using CV of (A) the ChOx/RGO/ITO bioelectrode as a function of cholesterol concentrations (25–500* mg $dL^{-1}$*); (B) Fitted calibration plot between anodic peak current and cholesterol concentrations for RGO (50-500* mg $dL^{-1}$*); (C) Electrochemical response studies of the ChOx/RGO-Fn Au NPs /ITO bioelectrode as a function of cholesterol concentrations (25–500* mg $dL^{-1}$*); (D) Fitted calibration plot for RGO-Fn Au NPs (25-500* mg $dL^{-1}$*).*

**Table.1**

*Comparison Table of sensing performances of different electrochemical biosensors for the determination of cholesterol:*

| System No. | Electrode material | Determination method | Detection Range (mM) | Detection Limit (mM) | Sensitivity ($\mu A\ mM^{-1}$) | $K_m$ value (mM) | Stability (days) | Reff. |
|---|---|---|---|---|---|---|---|---|
| Present Work | Ch-Ox/ RGO-Fn Au NPs | Amperometric | 0.65-12.93 | 0.33 | 193.3 | 0.005 | 9 weeks | Present work |
| Present Work | Ch-Ox/RGO | Amperometric | 1.3-12.93 | 0.26 | 116 | 0.01 | 6 weeks | Present work |
| System 1 | Cu2S NRS/CRIE | Amperometric | 0.01 - 6.8 | 0.0001 | 62.5 | - | 30 days 92.5% | [38] |
| System 2 | PEO-co-PPy/ChOx/Pt foil | Amperometric | - | - | 13.32 | 1.47 | 30 days | [39] |
| System 3 | AuPt–Ch–IL/GCE | Amperometry | 0.05–6.2, 6.2–11.2 | 0.01 | 90.7 | 0.24 | 30 days 90% | [40] |
| System 4 | MWCNT–chitosan–Pt–cholesterol | Amperometry | 0.005–0.3 | 0.004 | 44 | - | 7 days 60% | [41] |
| System 5 | Ti/NPAu/ChOx–HRP–ChE | CV | 0.97–7.8 | 0.012 | 29.33 | 0.64 | 60 days, 95% | [2] |
| System 6 | ITO(PEI/Hb)5 (PEI/COx)10, | Amperometric | - | 0.016 | 93.4 | - | 15 days | [42] |
| System 7 | (PAH–MCNTs–GNPs/HRP)4/(PAH–MCNTs–GNPs/ChOx)4 | CV | 0.18–11 | 0.02 | 0.3873 | - | 25 days 90% | [43] |
| System 8 | G/PVP/PANI nanocomposites | Amperometry | 0.05–10 | 0.001 | 34.77 | - | 14 days 89.1% | [44] |
| System 9 | AuE/dithiol/AuNPs/MUA/ ChOx | CV | 0.04–0.22 | 0.034 | 9.02 | 0.062 | 30 days 95% | [45] |
| System 10 | $NiFe_2O_4$/CuO/FeO-Ch/ChOx | DPV | 0.13–12.95 | 0.81067 | 16.54 | 0.21 | 90 days | [46] |

Note: DPV-differential pulse voltametery, NRS- nanostructure, CRIE- Cu rod integrated electrode, PEO-co-PPy-poly(ethyleneoxide)/polypyrrole, Ch-chitosan, IL- ionic liquid, GCE- glassy carbon electrode, HRP- horseradish peroxidase, PEI-poly(ethylene imine), Hb- hemoglobin, PAH- poly(allylamine hydrochloride), MCNTs- Multiwalled carbon nanotubes, G- graphene, PANI- polyaniline, PVP- polyvinylpyrrolidone, GNPs and Au NPs- gold nanoparticles, MUA- 11-mercaptoundecanoic acid.

Table 1 attests better sensing parameters of proposed RGO-Fn Au NPs/ITO matrix as compared to the RGO/ITO system and the earlier reported data for various matrix. The table places our electrode apart when compared to several types of materials system. Clearly, the earlier reported metal/ metal oxide nanostructure based systems (System 3, 5, 9 and 10) were much better in $K_m$ value than that of metal-polymer based system (System 2) but our RGO-Fn Au NPs/ITO system beats the metal/ metal oxide nanoparticles systems itself by an order of two in $K_m$ value, thus attesting its good affinity for bioanalytes. Similarly, the comparison of sensitivity shows that our RGO-Fn Au NPs/ITO system beats metal/ metal oxide nanostructures system (System 1, 3, 5, 9 and 10), carbon –metal nanostructure system (System 4), and metal- carbon – polymer nanostructured system (System 7) by an order of one. Further, it beats polymer based system (System 6) by an order of three and carbon – polymer nanostructured system (System 8) by an order of two. This, attests the systems commendable sensitivity in cholesterol detection. Moving ahead, the system has good detection range covering normal plus excess level of cholesterol usually found in human systems. Simultaneously, the detection limit although not very low but is more than enough to cover cholesterol range found in human systems. Thus, we have a sensor which can load analytes better (better $K_m$ value), detect appreciable range of cholesterol (good detection range), and does this at an enhanced rate (better $K_s$ value), while promising great stability of about 9 weeks. These enhanced sensing parameters owing to the combination of large surface area of the RGO and conductive nature of gold nanoparticle's, when combined with good biocompatibility and surface adsorbtion properties results in an commendable electrocatalytic system for cholesterol detetction.

## CONCLUSIONS

By way of conclusion, the present work reports RGO-Fn Au NPs hybrid system as a promising electrode platform for the electrochemical sensing of free cholesterol. Both the materials and the chemical synthesis route used are economical and the products have been well characterized by XRD, SEM, FTIR and Raman mapping. Bioelectrodes were fabricated by depositing thin films of RGO as well as RGO-Fn Au NPs on separate ITO substrates via cost effective and fast EPD technique, having potential for bulk production. To attain maximum efficiency restacking of RGO was resisted by immobilizing with ChOx after EDC-NHS coupling. Comparative electrochemical sensing study of these bioelectrodes confirms synergistically enhanced sensing ability of the newly proposed RGO-Fn Au NPs hybrid system over the traditional RGO system. Cyclic Voltametric study

shows that when used alone, RGO's sensitivity is limited to 116 μA $mM^{-1}$ $cm^{-2}$, however, when coupled with nanoparticles of Au, the resulting RGO-Fn Au NPs hybrid system shows much higher sensitivity of 193.35 μA $mM^{-1}$ $cm^{-2}$ when tested for the same range of cholesterol. These experimental findings have been corroborated by density functional theoretical (DFT) calculations using Gaussian09 software which attests enhanced electron density distribution in case of RGO-Fn Au NPs hybrid system. Further, the composite formation also favourably increases the chemical stability to about nine weeks, with good reproducibility and biocompatbility. Additionally, these enhanced sensing and stability benefits are achieved economically, with a single hybrid system based bioelectrode costing just ~0.2$. Thus, the proposed RGO-Fn Au NPs hybrid system shows promising potential to be used on field for $H_2O_2$ sensing, enabling critical clinical diagnostics.

**Acknowledgements**

SA is thankful to University Grants Commission, New Delhi; Institute of Physical Chemistry, Jena, Germany and Alexander von Humboldt for necessary facilities and financial support. Authors are thankful to the laboratories of Prof. Sebastian Schlucker, University of Duisburg, Essen, Germany and Dr. Valerian Ciobota, Rigaku Raman Technologies, Berlin, Germany for some of the characterizations. Authors are thankful to Dr. Vellaichamy Ganesan and Pankaj K Rastogi, Department of Chemistry, B.H.U. for EIS measurements.

**REFERENCES**

1. J. Motonaka and L. R. Faulkner, *Anal. Chem.*, 1993, **65**, 3258–3261.
2. A. Ahmadalinezhad and A. Chen, *Biosens. Bioelectron.*, 2011, **26**, 4508–4513.
3. M. Zhang, R. Yuan, Y. Chai, C. Wang, and X. Wu, *Anal. Biochem.*, 2013, **436**, 69–74.
4. S. Brahim, D. Narinesingh, and A. Guiseppi-Elie, *Anal. Chim. Acta*, 2001, **448**, 27–36.
5. B. Unnikrishnan, S. Palanisamy, and S.-M. Chen, *Biosens. Bioelectron.*, 2013, **39**, 70–75.
6. A.-L. Liu, G.-X. Zhong, J.-Y. Chen, S.-H. Weng, H.-N. Huang, W. Chen, L.-Q. Lin, Y. Lei, F.-H. Fu, and Z. Sun, *Anal. Chim. Acta*, 2013, **767**, 50–58.
7. S. Abraham, V. Ciobota, S. Srivastava, S. K. Srivastava, R. K. Singh, J. Dellith, B. D. Malhotra, M. Schmitt, J. Popp, and A. Srivastava, *Anal. Methods*, 2014, **6**, 6711–6720.
8. T. R. Tshikhudo, Z. Wang, and M. Brust, *Mater. Sci. Technol.*, 2004, **20**, 980–984.

9. P. Ghosh, G. Han, M. De, C. K. Kim, and V. M. Rotello, *Adv. Drug Deliv. Rev.*, 2008, **60**, 1307–1315.

10. R. A. Sperling, P. R. Gil, F. Zhang, M. Zanella, and W. J. Parak, *Chem. Soc. Rev.*, 2008, **37**, 1896–1908.

11. X. Huang, P. K. Jain, I. H. El-Sayed, and M. A. El-Sayed, 2007.

12. K. S. Novoselov, A. K. Geim, S. V Morozov, D. Jiang, Y. Zhang, S. V Dubonos, I. V Grigorieva, and A. A. Firsov, *Sci.* , 2004, **306** , 666–669.

13. M. Pumera, *Chem. Soc. Rev.*, 2010, **39**, 4146–4157.

14. J. Wei, J. Qiu, L. Li, L. Ren, X. Zhang, J. Chaudhuri, and S. Wang, *Nanotechnology*, 2012, **23**, 335707.

15. M. Zhou, Y. Zhai, and S. Dong, *Anal. Chem.*, 2009, **81**, 5603–5613.

16. Q. Xu, S.-X. Gu, L. Jin, Y. Zhou, Z. Yang, W. Wang, and X. Hu, *Sensors Actuators B Chem.*, 2014, **190**, 562–569.

17. S. Cao, L. Zhang, Y. Chai, and R. Yuan, *Biosens. Bioelectron.*, 2013, **42**, 532–538.

18. S. Abraham, V. Ciobota, S. K. Srivastava, R. K. Singh, J. Dellith, B. D. Malhotra, M. Schmitt, J. Popp, and A. Srivastava, *Anal. Methods*, 2014.

19. Y. Yan, Q. Liu, K. Wang, L. Jiang, X. Yang, J. Qian, X. Dong, and B. Qiu, *Analyst*, 2013, **138**, 7101–7106.

20. X. Bai and K.-K. Shiu, *J. Electroanal. Chem.*, 2014, **720**, 84–91.

21. K.-J. Huang, D.-J. Niu, X. Liu, Z.-W. Wu, Y. Fan, Y.-F. Chang, and Y.-Y. Wu, *Electrochim. Acta*, 2011, **56**, 2947–2953.

22. W. Hong, H. Bai, Y. Xu, Z. Yao, Z. Gu, and G. Shi, *J. Phys. Chem. C*, 2010, **114**, 1822–1826.

23. Y. Xue, H. Zhao, Z. Wu, X. Li, Y. He, and Z. Yuan, *Biosens. Bioelectron.*, 2011, **29**, 102–108.

24. D. C. Marcano, D. V Kosynkin, J. M. Berlin, A. Sinitskii, Z. Sun, A. Slesarev, L. B. Alemany, W. Lu, and J. M. Tour, *ACS Nano*, 2010, **4**, 4806–4814.

25. D. Li, M. B. Müller, S. Gilje, R. B. Kaner, and G. G. Wallace, *Nat. Nanotechnol.*, 2008, **3**, 101–105.

26. J. Liu and Y. Lu, *Nat. Protoc.*, 2006, **1**, 246–252.

27. Y.-W. Liu, M.-X. Guan, L. Feng, S.-L. Deng, J.-F. Bao, S.-Y. Xie, Z. Chen, R.-B. Huang, and L.-S. Zheng, *Nanotechnology*, 2013, **24**, 25604.

28. A. R. Biris, S. Pruneanu, F. Pogacean, M. D. Lazar, G. Borodi, S. Ardelean, E. Dervishi, F. Watanabe, and A. S. Biris, *Int. J. Nanomedicine*, 2013, **8**, 1429.

29. A. C. Ferrari, J. C. Meyer, V. Scardaci, C. Casiraghi, M. Lazzeri, F. Mauri, S. Piscanec, D. Jiang, K. S. Novoselov, S. Roth, and A. K. Geim, *Phys. Rev. Lett.*, 2006, **97**, 187401.

30. K. N. Kudin, B. Ozbas, H. C. Schniepp, R. K. Prud'Homme, I. A. Aksay, and R. Car, *Nano Lett.*, 2008, **8**, 36–41.

31. L. M. Malard, M. A. Pimenta, G. Dresselhaus, and M. S. Dresselhaus, *Phys. Rep.*, 2009, **473**, 51–87.

32. D. A. C. Brownson, S. A. Varey, F. Hussain, S. J. Haigh, and C. E. Banks, *Nanoscale*, 2014, **6**, 1607–1621.

33. Y. Hao, Y. Wang, L. Wang, Z. Ni, Z. Wang, R. Wang, C. K. Koo, Z. Shen, and J. T. L. Thong, *small*, 2010, **6**, 195–200.

34. J. E. B. Randles, *Discuss. Faraday Soc.*, 1947, **1**, 11–19.

35. P. Zanello, *Inorganic electrochemistry: theory, practice and applications*, Royal Society of Chemistry, 2003.

36. R. J. Klingler and J. K. Kochi, *J. Phys. Chem.*, 1981, **85**, 1731–1741.

37. H. Lineweaver and D. Burk, *J. Am. Chem. Soc.*, 1934, **56**, 658–666.

38. R. Ji, L. Wang, G. Wang, and X. Zhang, *Electrochim. Acta*, 2014.

39. H. B. Yildiz, D. O. Demirkol, S. Sayin, M. Yilmaz, O. Koysuren, and M. Kamaci, *J. Macromol. Sci. Part A*, 2013, **50**, 1075–1084.

40. A. Safavi and F. Farjami, *Biosens. Bioelectron.*, 2011, **26**, 2547–2552.

41. Y.-C. Tsai, S.-Y. Chen, and C.-A. Lee, *Sensors Actuators B Chem.*, 2008, **135**, 96–101.

42. T. T. L. Souza, M. L. Moraes, and M. Ferreira, *Sensors Actuators B Chem.*, 2013, **178**, 101–106.

43. X. Cai, X. Gao, L. Wang, Q. Wu, and X. Lin, *Sensors Actuators B Chem.*, 2013, **181**, 575–583.

44. N. Ruecha, R. Rangkupan, N. Rodthongkum, and O. Chailapakul, *Biosens. Bioelectron.*, 2014, **52**, 13–19.

45. U. Saxena, M. Chakraborty, and P. Goswami, *Biosens. Bioelectron.*, 2011, **26**, 3037–3043.

46. J. Singh, M. Srivastava, P. Kalita, and B. D. Malhotra, *Process Biochem.*, 2012, **47**, 2189–2198.